Material design of indium-based compounds: Possible candidates for charge, valence, and bond disproportionation and superconductivity

Chang-Jong Kang and Gabriel Kotliar

Material design of indium based compounds: possible candidates for charge, valence, and bond disproportionation and superconductivity

Chang-Jong Kang[1]* and Gabriel Kotliar[1,2]

[1]*Department of Physics and Astronomy, Rutgers University, Piscataway, New Jersey 08854, USA*
[2]*Condensed Matter Physics and Materials Science Department,*
Brookhaven National Laboratory, Upton, New York 11973, USA
(Dated: December 13, 2018)

We design and investigate the physical properties of new indium compounds $AInX_3$ (A = alkali metals, X = F or Cl). We find nine new In based materials in their ground state and are thermodynamically stable but are not reported in ICSD (Inorganic Crystal Structure Database). We also discuss several metastable structures. This new series of materials display multiple valences, charge and bond disproportionation, and dimerization. The most common valence of In is 3+. We also find two rare alternatives, one has In^{2+} with In-In dimerization and the other shows valence disproportionation to In^{1+} and In^{3+} with bond disproportionation. We study the possibility of superconductivity in these new In compounds and find that $CsInF_3$ has a transition temperature about 24 K with sufficient hole doping and pressure.

I. INTRODUCTION

Progress in theory and algorithms, coupled with increased computational power is now accelerating the discovery of new materials with useful physical properties. A notable recent success is the theory led discovery of high temperature superconductivity of hydrogen sulfide under pressure[1–5], which has set the record of the highest critical temperature reached so far. Other examples of recent predictions are existence of a metallic layer in a new family (112) of iron based superconductors[6–8], the prediction and synthesis of missing half-Heusler compounds[9–11], the prediction of new high-pressure phase materials such as FeO_2[12], calcium carbides[13], and Na_2He[14], which were also confirmed experimentally. For reviews see Refs.[15–20]. Theory and computation are thus beginning to play a decisive role in the search for new materials.

In this paper we apply material design methodology to find new indium halide compounds. There are multiple motivations for this study. One is the intrinsic interest in finding new mixed valent compounds, a condition that is very rare in the solid state, but has been a focus on interest for many years[21]. With an eye on possible applications, halide perovskites, such as $CsPbI_3$[22], are remarkable photovoltaic[23,24] materials. They have also been studied as analogs, as they have very similar band structures[25,26] of the high temperature superconductor $BaBiO_3$[27]. Another motivation is to make predictions in a new arena that will test a material design methodology, which assigns a likelihood that a material will form.

Indium compounds tend to form in an oxidation state of In^{3+}, and the valences In^{1+} and In^{2+} are not typical[28–30]. We find nine new indium fluoride/chloride compounds where indium is in a valence 2+ or 1+, which have a very high probability to form within the framework of Adler *et al.*[31] and are thermodynamically stable within the density functional theory PBE (Perdew-Burke-Ernzerhof) functional. For a given composition we identify potential low-energy crystal structures for the indium fluoride/chloride compounds, as candidate structures and find the relation between the crystal structure and the valence state of indium. These indium fluoride/chloride compounds display multiple valences, charge and bond disproportionation, and indium-indium dimerization. The new indium fluoride/chloride compounds have too large of a band gap (of the order of ∼4 eV) to be useful for photovoltaic materials, but could be useful for other applications. In particular, hole-doped $CsInF_3$ under pressure will exhibit superconductivity with transition temperature of 24 K.

II. OUTLINE

In the beginning, we would like to summarize a material design workflow introduced in Ref. [31]. The material design process is initiated by the **qualitative ideas** including some physical idea of a model that one would like to explore or test, ways to enhance desirable physical properties of a material, and comparisons of a class of compounds that exhibit the similar physical properties. The initial intuitions (zeroth order step) could be refined with simplified quantitative calculations using a model Hamiltonian or other computational tools like *ab initio* density functional theory (DFT). In this work, we have used DFT as a main computational tool to design a new material. Note that the "theoretical" material design workflow progresses in reverse order from experimental solid state synthesis.

The first step is the quantitative calculation of the **electronic structure**. It explores how to go from a well defined crystal structure of a material to exhibit physical or chemical properties. The second step is a **prediction of the crystal structure** given a fixed chemical composition. There are a number of structure prediction techniques[32] with DFT total energy calculations, and the prediction techniques require having an accurate method for calculating the total energy of a material in the DFT level. The third step is testing for **thermodynamic**

stability: given the lowest energy crystal structure of the fixed composition, check whether it is stable against decomposition to all other compositions in the chemical system. The third step requires the knowledge of all other known stable compositions, their crystal structures and total energies, which is now facilitated by materials databases, such as Materials Project[33,34], OQMD[35,36], and AFLOWlib[37,38]. Here, we have used the Materials Project database for analysis of thermodynamic stability and estimated the existence probability[31] based on the database.

Once the (thermodynamically) stable crystal structure is found, the electronic structure is calculated again with more elaborated DFT methods like hybrid functionals, the modified Becke-John (mBJ) exchange potential, and GW methods to obtain more accurate physical properties.

This paper is organized as follows: the detail computational method of each step for material design is provided in Sec. III. The computational results are presented in sequence of the material design workflow. Section IV A summarizes the initial qualitative idea (zeroth order step) and its validation (first step). The prediction of crystal structures (second step) of the indium halide compounds and their thermodynamic stabilities (third step) are presented in Sec. IV B and Sec. IV C, respectively. The details of electronic structures and superconducting properties (post-process) are provided in Sec. IV D. The paper closes with brief summary and conclusions in Sec. V.

III. METHOD

A. Prediction of crystal structure

To obtain low-energy crystal structures of $AInX_3$ (A = alkali metals, X = F or Cl), we employed the *ab initio* evolutionary algorithm[39] implemented in USPEX[40] combined with DFT pseudopotential code VASP[41,42]. The initial structures were randomly generated according to possible space groups. In these calculations, the structural optimization of all the newly generated structures were carried out by VASP with an energy cutoff of 520 eV and the exchange-correlation functional of generalized gradient approximation (GGA) of Perdew-Burke-Ernzerhof (PBE)[43] with the projector augmented wave (PAW) method[44,45].

B. Thermodynamic stability

After low-energy crystal structures were obtained, corresponding total energies were calculated by using DFT pseudopotential code VASP[41,42]. For the Brillouin-zone integration, the equal k-grid density was used for all materials by adopting the Monkhorst-Pack sampling grid with a reciprocal spacing of 64 k-points per Å^{-1}. We

used the empirical correction schemes employed in Materials Project[31,33,46–49] to get an accurate formation energy. In addition, the Materials Project database was used for analysis of thermodynamic stability and the existence probability[31].

C. Electronic structure

The all-electron full-potential linearized augmented plane-wave (FP-LAPW) method implemented in WIEN2k[50] was adopted to calculate the electronic structure. GGA(PBE) exchange-correlation functional was chosen to calculate the electronic structure. To get the precise band gap, we utilized the modified Becke-John (mBJ) exchange potential[51], which is rather accurate and computationally cheaper than GW method. The Brillounin zone integration was done with a $17{\times}17{\times}17$ k-mesh and the plane-wave cutoff was $R_{\mathrm{mt}}K_{\max} = 7$. The maximum L value for the waves inside the atomic spheres, $L_{\max} = 10$, and the largest G in the charge Fourier expansion $G_{\max} = 12$ were used in the calculations.

D. Phonon dispersion and electron-phonon coupling calculations

We used the linear response method[52] implemented in Quantum Espresso[53] for phonon calculations. All pseudopotentials used in the calculations were adopted from Standard Solid State Pseudopotentials[54,55]. We used a $10 \times 10 \times 10$ k-grid and a Gaussian smearing of 0.03 Ry for the electronic integration. The dynamical matrices were calculated on a $4 \times 4 \times 4$ phonon-momentum grid. A $20 \times 20 \times 20$ k-grid was used for the electron-phonon coupling calculations. The standard exchange-correlation functionals like local-density approximation (LDA) and generalized gradient approximation (GGA) neglect the long-range exchange interaction. This nonlocal correlation could play an significant role in electron-phonon interaction[56]. To incorporate the long-range exchange interaction, the Heyd-Scuseria-Ernzerhof hybrid functional (HSE06)[57] was used and the electron-phonon coupling constant was calculated from the HSE06 deformation potential introduced in Ref. [56].

IV. COMPUTATIONAL RESULTS AND DISCUSSION

A. Initial idea and its validation

We conceived the idea that new indium halide compounds have physical and chemical similarities with $BaBiO_3$[27], a high temperature superconductor, and $CsPbI_3$[22], a high performance photovoltaic material. To
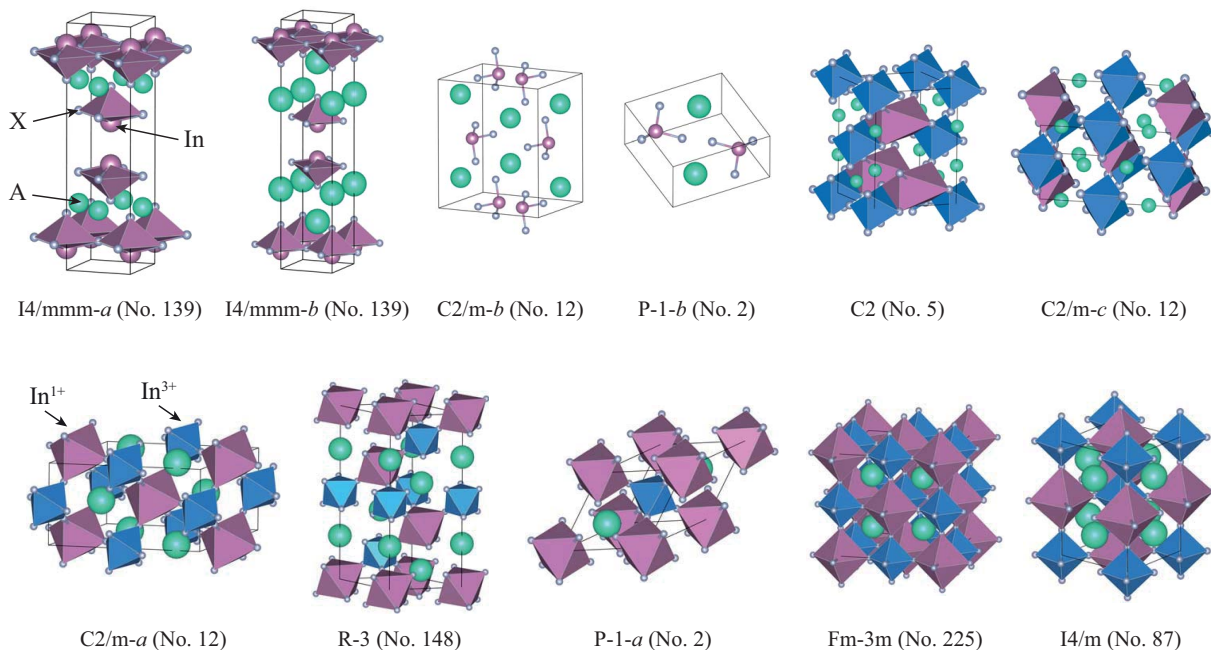
FIG. 1. (Color Online) Possible candidates for low-energy crystal structures of $AInX_3$ (A = alkali metals, X = F or Cl) obtained by USPEX simulations. Space groups are also provided below for each crystal structure. Structures listed in the second row could be identified from structural distortions (breathing and/or tilting of InX_6 octahedra) in the ideal cubic perovskite structure. For the structures, octahedra centered at In^{3+} or In^{1+} are colored in navy or pink, respectively. Letters a, b, and c are attached to the end of the space group notation if different crystal structures have the same space group.

justify the initial idea briefly, we assumed that new indium halide compounds have the ideal cubic perovskite structure. To get an unknown lattice constant of the perovskite structure, we performed the structural relaxation with VASP. After obtaining the relaxed crystal structures for the indium halide compounds, the electronic structures were obtained from the DFT calculations. Comparing the electronic structures, we could conclude that the indium halide compounds have similar physical properties exhibited in $BaBiO_3$ and $CsPbI_3$. Therefore, the indium halide compounds could be possible candidates for high-temperature superconductors or photovoltaic materials.

B. Crystal structure and total energy profile

The possible candidates for low-energy crystal structures of $AInX_3$ (A = alkali metals, X = F or Cl) obtained by USPEX are summarized in Fig. 1[58].

The crystal structures having the lowest energy are tetragonal structures with space group $I4/mmm$ (No. 139) for $AInF_3$ (A = Li, Na, K, and Rb) (see Fig. 2) however, Wyckoff sites for A are different: $4d$ for both Li and Na, and $4e$ for both K and Rb. Therefore, we have labeled the space group $I4/mmm$ having two different Wyckoff sites $4d$ and $4e$ with $I4/mmm$-a and $I4/mmm$-b, respectively, in order to distinguish different crystal structures with the same space group. The coordination

number of In in $I4/mmm$-$AInF_3$ (A = Li, Na, K, and Rb) is 5 that makes a InF_5 pyramid (Fig. 1). Alkali metal A and F strongly have 1+ and 1- valence states, respectively, hence In should have 2+ valence state in order for the system to be charge neutral. The 2+ valence state for In is very unique because In usually has 3+ valence state.

For $CsInF_3$, five space groups $C2/m$-a, $R\bar{3}$, $P\bar{1}$-a, $Fm\bar{3}m$, and $I4/m$ are candidates for the lowest energy structure and have tiny energy differences within 1 meV/atom (which corresponds to ∼10 K in temperature) to each other (Fig. 2). The details of the energy differences could be found in Table I. They could be identified from structural distortions (breathing and/or tilting of InF_6 octahedra) in the ideal cubic perovskite structure and have different sizes of InF_6 octahedra (Fig. 1). One has short In-F bond length (∼2.12 Å) and it leads for In having 3+ valence state. On the other hand, the other has long In-F bond length (∼2.68 Å) and it results in In 1+ valence state. Therefore, the different In-F bond lengths (bond disproportionation) trigger charge/valence disproportionation. We would like to note that the crystal structure of $CsInF_3$ with the space group $C2/m$-a is quite similar to that of $BaBiO_3$, which has also the monoclinic structure with a space group $C2/m$ at low temperature[59–61]. For $BaBiO_3$, the Bi atoms occupy two distinct Wyckoff sites with average Bi-O distances of 2.28 and 2.12 Å, respectively[59], and results in valence disproportionation of Bi^{3+} and Bi^{5+}[61,62].
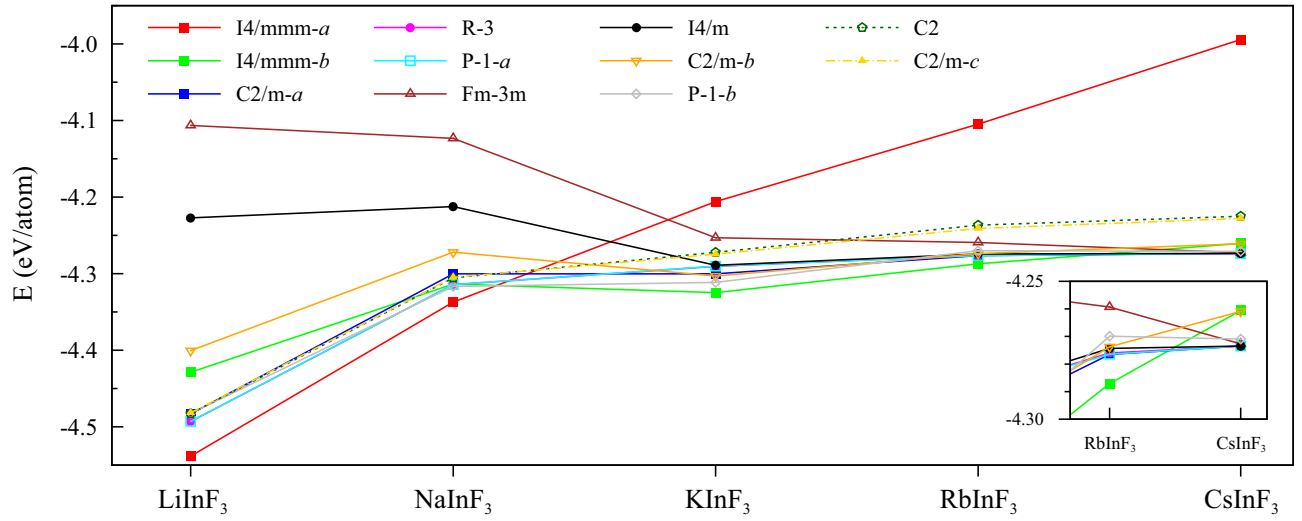
FIG. 2. (Color Online) Total energies of crystal structures listed in Fig. 1 for AInF$_3$ (A = alkali metals). Inset is provided to zoom in for nearly degenerate phases of RbInF$_3$ and CsInF$_3$. The space group $I4/mmm$-a is the ground state crystal structure for both LiInF$_3$ and NaInF$_3$, and $I4/mmm$-b is for both KInF$_3$ and RbInF$_3$. For CsInF$_3$, five space groups ($C2/m$-a, $R\bar{3}$, $P\bar{1}$-a, $Fm\bar{3}m$, and $I4/m$) are candidates for the lowest energy structure and are almost degenerate. The energy differences among the five space groups are within 1 meV/atom.
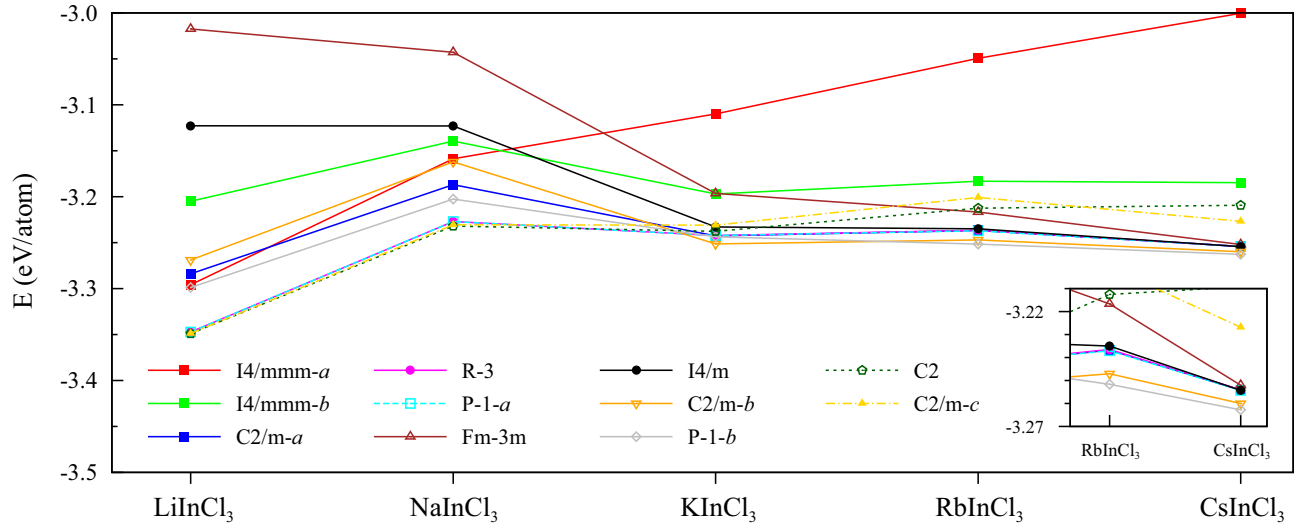

FIG. 3. (Color Online) Total energies of crystal structures listed in Fig. 1 for AInCl$_3$ (A = alkali metals). Inset is provided to zoom in for nearly degenerate phases of RbInCl$_3$ and CsInCl$_3$. Four space groups, $R\bar{3}$, $P\bar{1}$-a, $C2$, and $C2/m$-c, are candidates for the lowest energy structure of LiInCl$_3$ and NaInCl$_3$, and energy differences among the four space groups are within 5 meV/atom. For KInCl$_3$, RbInCl$_3$, and CsInCl$_3$, two space groups, $C2/m$-b and $P\bar{1}$-b, are candidates for the lowest energy structure, and energy differences between the two space groups are within 9 meV/atom.

The crystal structure with the space group $I4/mmm$-a has the lowest energy for LiInF$_3$ and NaInF$_3$ however, it has higher energy as alkali metal gets heavier as shown in Fig. 2. The other crystal structures listed in Fig. 1 have significant energy differences among them in LiInF$_3$ but these energy differences go smaller as alkali metal becomes heavier. For CsInF$_3$, these energy differences are within 13 meV/atom and energy differences among five candidate structures (with space groups $C2/m$-a, $R\bar{3}$,

$P\bar{1}$-a, $Fm\bar{3}m$, and $I4/m$) are only within 1 meV/atom. The energy difference between the lowest and the next lowest energy is gradually reduced as alkali metal becomes heavier: 45, 20, 13, 11, and 0.01 meV/atom for Li, Na, K, Rb, and Cs compounds, respectively (see Table I). Judging from these energy differences, AInF$_3$ is likely synthesized into the space group $I4/mmm$-a for both Li and Na and $I4/mmm$-b for both K and Rb compounds if they are thermodynamically stable (their ther-
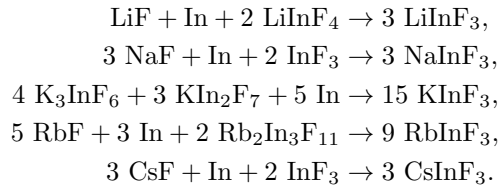
modynamic stabilities will be discussed later on). However, synthesis of $CsInF_3$ quite depends on the synthesis method and condition due to the quite small energy difference. It could be one of five candidate structures (with space groups $C2/m$-a, $R\bar{3}$, $P\bar{1}$-a, $Fm\bar{3}m$, and $I4/m$) depending on the synthesis condition. Or otherwise, it exists in several different polymorphs. Note that charge-ordered thallium halide perovskites $CsTlX_3$ (X = F or Cl) is successfully synthesized. $CsTlF_3$ has a cubic phase ($Fm\bar{3}m$). On the other hand, $CsTlCl_3$ exists in two different polymorphs: a tetragonal phase ($I4/m$) and a cubic phase ($Fm\bar{3}m$)[25].

The possible candidates for low-energy crystal structures of $AInCl_3$ have been also investigated along with $AInF_3$. Since fluorine and chlorine atoms belong to the same halogen group in the periodic table, $AInCl_3$ is expected to have close resemblances to $AInF_3$ structurally and electronically. To check the possible low-energy crystal structures for $AInCl_3$, we examined total energies of the crystal structures listed in Fig. 1 and the results are shown in Fig. 3. For both $LiInCl_3$ and $NaInCl_3$, four space groups, $R\bar{3}$, $P\bar{1}$-a, $C2$, and $C2/m$-c, are candidates for the lowest energy structure and have tiny energy differences only within 5 meV/atom. The details of the energy differences could be found in Table II. These four space groups, $R\bar{3}$, $P\bar{1}$-a, $C2$, and $C2/m$-c, possess two different sizes of $InCl_6$ octahedra (bond disproportionation, see Fig. 1). It leads for In to have In^{1+} and In^{3+} valence states and shows charge/valence disproportionation. For $AInCl_3$ (A = K, Rb, Cs), two space groups, $C2/m$-b and $P\bar{1}$-b, are candidates for the lowest energy structure. Energy differences between the two space groups are 7.8, 4.6, and 2.8 meV/atom for K, Rb, and Cs compounds, respectively (see Table II). These two space groups possess symmetrically equivalent In atoms in the unit cell, hence charge/valence disproportionation is not available for the space groups (bond disproportionation is not available as well). The coordination number of In in both $C2/m$-b and $P\bar{1}$-b space groups is 3, which is quite distinct from the others listed in Fig. 1. The space group $I4/mmm$-a has higher energy as alkali metal gets heavier as shown in Fig. 3. Besides, energy differences among space groups except for $I4/mmm$-a are significant for $LiInCl_3$ and go smaller as alkali metal becomes heavier. These two tendencies are also realized in $AInF_3$ compounds (Fig. 2).

C. Thermodynamic stability

We construct the ternary phase diagrams for $AInF_3$ compounds as shown in Fig. 4. All lowest-energy $AInF_3$ compounds are thermodynamically stable (Table I). The

determinant reactions for $AInF_3$ are

$$LiF + In + 2\,LiInF_4 \rightarrow 3\,LiInF_3,$$
$$3\,NaF + In + 2\,InF_3 \rightarrow 3\,NaInF_3,$$
$$4\,K_3InF_6 + 3\,KIn_2F_7 + 5\,In \rightarrow 15\,KInF_3,$$
$$5\,RbF + 3\,In + 2\,Rb_2In_3F_{11} \rightarrow 9\,RbInF_3,$$
$$3\,CsF + In + 2\,InF_3 \rightarrow 3\,CsInF_3.$$

Given the above determinant reactions, we can estimate the energy above/below hull (E_{Hull}) for $AInF_3$ and the results are shown in Table I. Since all lowest-energy $AInF_3$ compounds have substantial energies below hull, they are most likely to form.

We are now in a position to discuss the possibility of synthesis of suggested $AInF_3$ materials. To do that, we made a probabilistic model to estimate the existence probability of a material[31]. If a material has a significant energy below hull, the existence probability becomes larger, indicating synthesis of the material would be likely possible. $LiInF_3$, $NaInF_3$, $KInF_3$, and $RbInF_3$ have energy below hull of -30, -54, -21, and -50 meV/atom, respectively, which correspond to the existence probability of 0.56, 0.64, 0.52, and 0.62, respectively. Since these existence probabilities are large enough, these $AInF_3$ compounds are expected to be synthesized in laboratory. Especially $CsInF_3$ phases have energies below hull of order of -100 meV/atom, which corresponds to the existence probability of 0.78. Since five candidate structures have small energy differences among them (within

TABLE I. Hull energy (E_{Hull}), energy difference (ΔE), and existence probability for the low-energy crystal structure of $AInF_3$ (A = alkai metals). The hull energy is obtained from the determinant reaction (see text), the energy difference is estimated with respect to the crystal structure having the lowest energy, and the existence probability is calculated by using the probabilistic model introduced in Ref. [31]. The units for E_{Hull} and ΔE are meV/atom.

Space group	E_{Hull} (meV)	ΔE (meV)	Prob.
	$LiInF_3$		
$I4/mmm$-a (No. 139)	-30.362	0	0.56
$R\bar{3}$ (No. 148)	14.860	45.222	0.39
	$NaInF_3$		
$I4/mmm$-a (No. 139)	-54.183	0	0.64
$P\bar{1}$-b (No. 2)	-33.838	20.345	0.57
	$KInF_3$		
$I4/mmm$-b (No. 139)	-20.501	0	0.52
$P\bar{1}$-b (No. 2)	-7.298	13.202	0.46
	$RbInF_3$		
$I4/mmm$-b (No. 139)	-49.727	0	0.62
$C2/m$-a (No. 12)	-39.139	10.588	0.59
$P\bar{1}$-a (No. 2)	-39.109	10.618	0.59
	$CsInF_3$		
$C2/m$-a (No. 12)	-115.011	0	0.78
$I4/m$ (No. 87)	-114.999	0.012	0.78
$R\bar{3}$ (No. 148)	-114.995	0.016	0.78
$P\bar{1}$-a (No. 2)	-114.983	0.028	0.78
$Fm\bar{3}m$ (No. 225)	-114.228	0.783	0.77
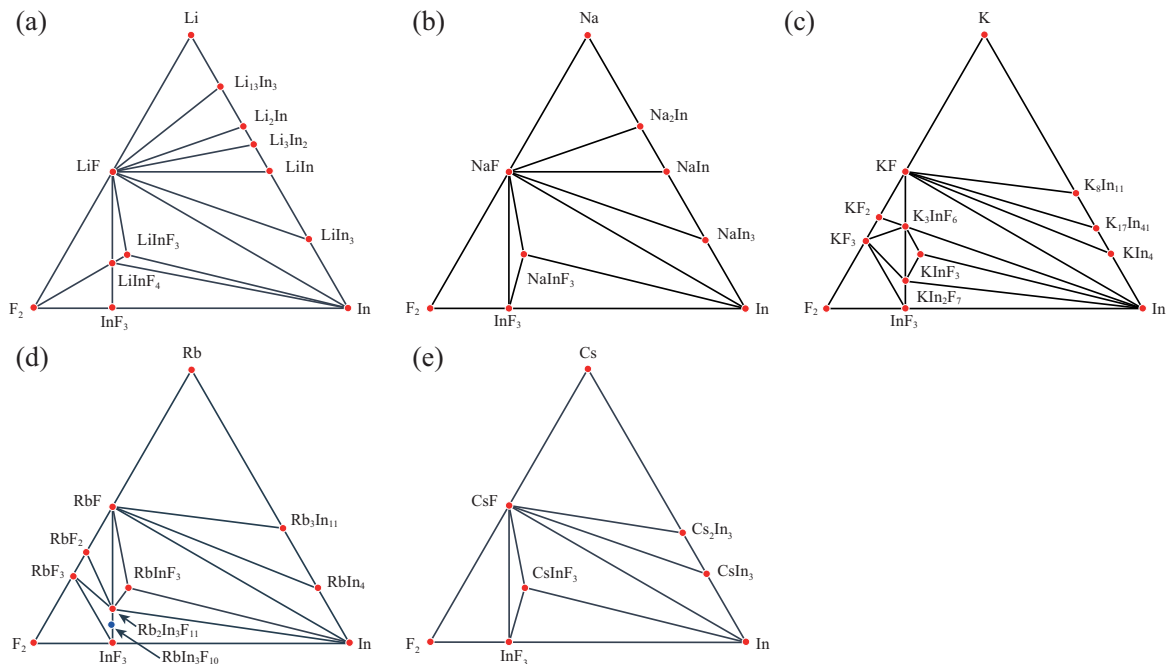
FIG. 4. (Color Online) Ternary phase diagrams for (a) LiInF$_3$, (b) NaInF$_3$, (c) KInF$_3$, (d) RbInF$_3$, and (e) CsInF$_3$. Note that RbIn$_3$F$_{10}$ is marginally stable with a tiny energy above hull of 1.26 meV/atom (existence probability of 0.43).

1 meV/atom), existence probabilities for the structures are almost same as 0.78 (see Table. I). As mentioned before, synthesis of the crystal structure quite depends on the synthesis method and condition. In the case of CsInF$_3$, one of five candidate structures would be chosen and synthesized depending on the synthesis condition. Or otherwise, it exists in several different polymorphs.

TABLE II. Same as Table. I for AInCl$_3$ compounds.

Space group	E_{Hull} (meV)	ΔE (meV)	Prob.
LiInCl$_3$			
$C2$ (No. 5)	-23.532	0	0.53
$C2/m$-c (No. 12)	-23.228	0.304	0.53
$R\bar{3}$ (No. 148)	-21.669	1.863	0.52
$P\bar{1}$-a (No. 2)	-21.648	1.885	0.52
NaInCl$_3$			
$C2$ (No. 5)	-4.727	0	0.45
$C2/m$-c (No. 12)	-3.410	1.316	0.45
$R\bar{3}$ (No. 148)	0.114	4.841	0.44
$P\bar{1}$-a (No. 2)	0.130	4.857	0.44
KInCl$_3$			
$C2/m$-b (No. 12)	0.617	0	0.43
$P\bar{1}$-b (No. 2)	8.450	7.833	0.41
RbInCl$_3$			
$P\bar{1}$-b (No. 2)	-79.011	0	0.70
$C2/m$-b (No. 12)	-74.430	4.581	0.69
CsInCl$_3$			
$P\bar{1}$-b (No. 2)	-20.112	0	0.52
$C2/m$-b (No. 12)	-17.336	2.776	0.51
$I4/m$ (No. 87)	-11.657	8.455	0.48

Figure 5 shows the ternary phase diagrams for AInCl$_3$ compounds. The determinant reactions for AInCl$_3$ are
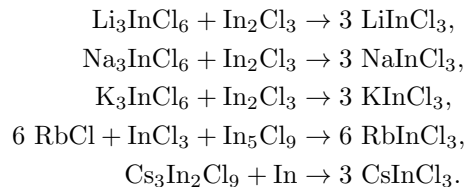
$$\text{Li}_3\text{InCl}_6 + \text{In}_2\text{Cl}_3 \rightarrow 3\,\text{LiInCl}_3,$$
$$\text{Na}_3\text{InCl}_6 + \text{In}_2\text{Cl}_3 \rightarrow 3\,\text{NaInCl}_3,$$
$$\text{K}_3\text{InCl}_6 + \text{In}_2\text{Cl}_3 \rightarrow 3\,\text{KInCl}_3,$$
$$6\,\text{RbCl} + \text{InCl}_3 + \text{In}_5\text{Cl}_9 \rightarrow 6\,\text{RbInCl}_3,$$
$$\text{Cs}_3\text{In}_2\text{Cl}_9 + \text{In} \rightarrow 3\,\text{CsInCl}_3.$$

Given the above determinant reactions, we can estimate the energy above/below hull (E_{Hull}) for AInCl$_3$ and the results are shown in Table II. All lowest-energy AInCl$_3$ compounds are thermodynamically stable except for KInCl$_3$. KInCl$_3$ has energy above hull of 0.617 meV/atom and the corresponding existence probability is 0.43, which is quite significant. Therefore, KInCl$_3$ is marginally stable and is still expected to be synthesized in laboratory. The other AInCl$_3$ compounds have energy below hull of -23, -4, -79, and -20 meV/atom for Li, Na, Rb, and Cs compounds, which correspond to the existence probability of 0.53, 0.45, 0.70, and 0.52, respectively. Since these existence probabilities are large enough, these AInCl$_3$ compounds are expected to be synthesized in laboratory. Both LiInCl$_3$ and NaInCl$_3$ have tiny energy differences (within 5 meV/atom) among four candidate space groups, $C2$, $C2/m$-c, $R\bar{3}$, and $P\bar{1}$-a. For RbInCl$_3$ and CsInCl$_3$, two candidate space groups, $P\bar{1}$-b and $C2/m$-b, also have tiny energy differences (within 5 meV/atom) between them. Therefore, AInCl$_3$ (A = Li, Na, Rb, Cs) could be synthesized into one of candidate structures depending on the synthesis condition. Or otherwise, they exist in several different polymorphs. For
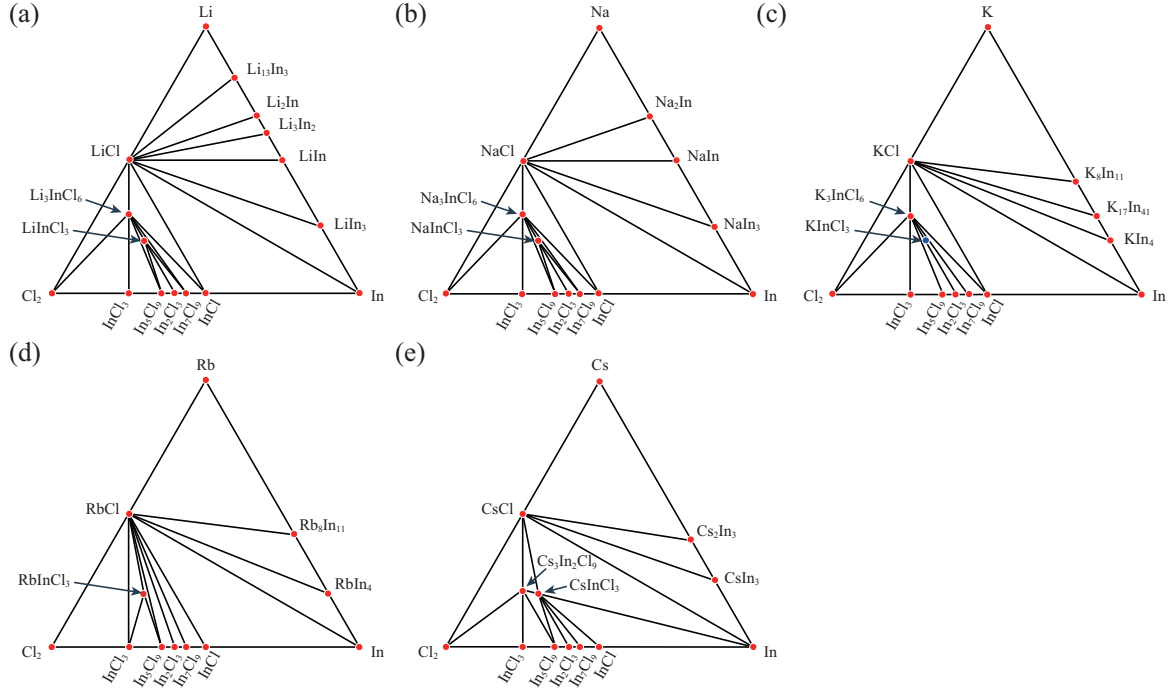
FIG. 5. (Color Online) Ternary phase diagrams for (a) LiInCl$_3$, (b) NaInCl$_3$, (c) KInCl$_3$, (d) RbInCl$_3$, and (d) CsInF$_3$. Red and blue filled circles represent thermodynamically stable and unstable phases, respectively. KInCl$_3$ is thermodynamically unstable with a quite small energy above hull of 0.617 meV/atom, which is marginally stable.

CsInCl$_3$, the third lowest-energy structure ($I4/m$) has a small energy difference of ∼8 meV with the lowest one and still has a possibility to form due to the considerable existence probability of 0.48 as shown in Table. II.

D. Electronic structure and superconductivity

We have calculated the electronic structures of AInF$_3$ compounds and found several similarities and differences among them. In Fig. 6, we present two representative electronic structures of $I4/mmm$-a LiInF$_3$ and $C2/m$-a CsInF$_3$. The similarities and differences in the electronic structures of AInF$_3$ will be discussed later.

Figure 6 shows that both LiInF$_3$ and CsInF$_3$ have the insulating phase with a indirect band gap of 4.37 and 4.06 eV, respectively, based on the mBJ method (GGA results give 2.30 and 3.05 eV, respectively). In addition, In s and F p orbitals are well separated in the energy window and it leads to small hybridization between In s and F p orbitals. The only notable hybridization is between In s and F p_σ orbitals and produces the low-lying bonding state located at -8 ∼ -6 eV as shown in Fig. 6. However, the low-lying bonding state has dominant F p_σ character and quite small In s character (see the density of states in Fig. 6). Due to the quite small hybridization between In s and F p orbitals, we can mention that LiInF$_3$ and CsInF$_3$ have In^{2+} ($5s^1$) and multivalent In^{1+} ($5s^2$) and In^{3+} ($5s^0$) configurations, respectively. We would like to note that charge disproportionation in

BaBiO$_3$[59,61] (2Bi^{4+} → Bi^{3+} + Bi^{5+}) was questioned due to the significant hybridization between Bi $6s$ and O $2p$ orbitals. The alternative scenario of oxygen hole pairs condensation (2Bi$^{3+}\underline{L}$ → Bi$^{3+}\underline{L}^2$ + Bi^{3+}, where $\underline{L}$ represents a ligand hole) was proposed[63–65]. In the case of CsInF$_3$, however, hybridization between In s and F p orbitals is quite small. Hence, the ligand hole pairs condensation scenario is safely ruled out and valence/charge disproportionation is clearly realized.

The electronic structures of other low-energy AInF$_3$ compounds including $I4/mmm$-a NaInF$_3$, $I4/mmm$-b KInF$_3$, and $I4/mmm$-b RbInF$_3$ (not shown) are quite similar to that of $I4/mmm$-a LiInF$_3$ except for the different size of the band gap. The sizes of the indirect band gap for Na, K, and Rb compounds obtained from the mBJ method are 3.89, 3.91, and 3.67 eV, (GGA results give 1.77, 1.90, and 1.90 eV), respectively, which are smaller than that for LiInF$_3$. For CsInF$_3$, the five candidate structures, which are $C2/m$-a, $I4/m$, $R\bar{3}$, $P\bar{1}$-a, and $Fm\bar{3}m$, also have the similar electronic structure in the following manners: (i) In s and F p orbitals are well separated in the energy window (In s and F p orbitals lie -1 ∼ 7 eV and -7 ∼ -4 eV, respectively), (ii) quite small hybridization between In s and F p orbitals is realized, (iii) multivalent In^{1+} ($5s^2$) and In^{3+} ($5s^0$) valence skip configuration is clearly shown, and (iv) the five candidate structures have the similar band gaps of ∼4.0 eV (GGA results give almost same band gaps of ∼3.0 eV).

Both $I4/mmm$-a LiInF$_3$ and $C2/m$-a CsInF$_3$ show the insulating behavior, however, the insulating mech-

anism is different (The insulating mechanism of the Na, K, and Rb compounds is essentially same as the Li compound). As shown in Fig. 6(b), $C2/m$-a CsInF$_3$ exhibits the mix-valent In^{1+} ($5s^2$) and In^{3+} ($5s^0$) character[66], where In^{1+} has the completely filled s-band and In^{3+} has the (nearly) empty s-band (there is small amount of In^{3+} s-orbital character in the occupied band due to the small hybridization between In s and F p_σ orbitals). Therefore, the insulating mechanism in $C2/m$-a CsInF$_3$ is straightforward: the mix-valent character makes the insulating phase. For the case of $I4/mmm$-a LiInF$_3$, In^{2+} ($5s^1$) character is clearly shown in Fig. 6(a), where In^{2+} has the half-filled s-band, which is not straightforward to understand the band gap formation. In order to investigate the insulating mechanism in $I4/mmm$-a LiInF$_3$ thoroughly, we plot the charge density with the energy range between -2 and 0 eV (the Fermi level is set to be zero) in Fig. 7(b), which corresponds to the $ss\sigma$-bonding character. Therefore, two adjacent In atoms are dimerized with the bond length of 2.75 Å to produce $ss\sigma$ (bonding) and $ss\sigma^*$ (anti-bonding) states, and each s-electron in In^{2+} completely fills the $ss\sigma$-bonding state (Fig. 7(a)). The band gap size in $I4/mmm$-a LiInF$_3$ indicates the splitting between $ss\sigma$ (bonding) and $ss\sigma^*$ (anti-bonding) states.

The electronic structures of all AInCl$_3$ compounds show the insulating behavior as well (not shown). AInCl$_3$ could be classified into two groups: LiInCl$_3$ and NaInCl$_3$ are in the same group and KInCl$_3$, RbInCl$_3$, and CsInCl$_3$ belong to the other group. For each group, they share
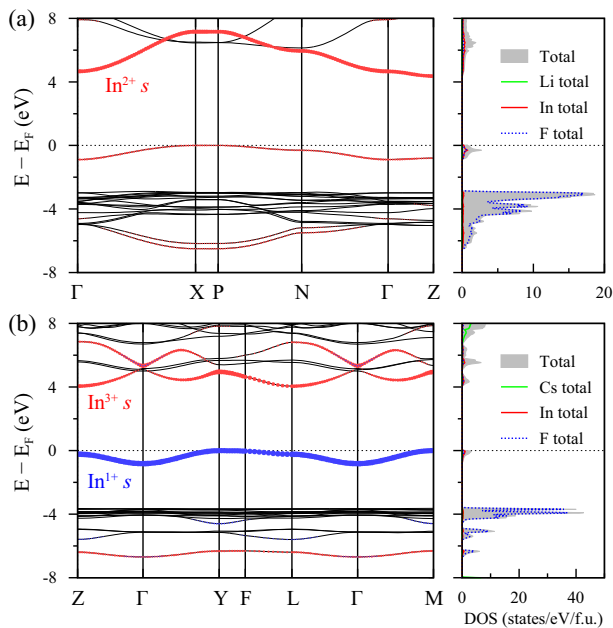

FIG. 6. (Color Online) Electronic structures of (a) $I4/mmm$-a LiInF$_3$ and (b) $C2/m$-a CsInF$_3$ calculated by the mBJ method. In^{2+} s-orbital character is marked in red in (a) and In^{3+} and In^{1+} s-orbital characters are marked in red and blue in (b), respectively, in the band structures.
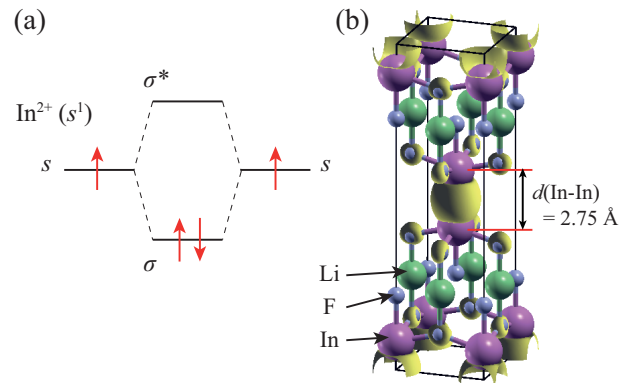

FIG. 7. (Color Online) Insulating mechanism of $I4/mmm$-LiInF$_3$. (a) Systematic band diagram for a band gap opening. Two s orbitals from two adjacent In^{2+} atoms form $ss\sigma$-bonding to open the band gap. (b) Electronic charge density corresponding to the $ss\sigma$-bonding. The distance between two adjacent In^{2+} atoms is 2.75 Å.

the same low-energy candidate structures: both LiInCl$_3$ and NaInCl$_3$ have the four candidate structures with space groups of $C2$, $C2/m$-c, $R\bar{3}$, and $P\bar{1}$-a, and KInCl$_3$, RbInCl$_3$, and CsInCl$_3$ have the two candidate structures with space groups of $P\bar{1}$-b and $C2/m$-b. Not only the electronic structures but also the size of the band gap are almost same among the candidate structures for each AInCl$_3$ compound. The band gaps obtained from the mBJ method are 3.5, 3.5, 4.2, 4.3, and 4.3 eV for Li, Na, K, Rb, and Cs compounds, respectively (GGA gives the band gaps of 2.8, 2.7, 2.9, 3.0, and 3.0 eV, respectively). For both LiInCl$_3$ and NaInCl$_3$, their four candidate structures possess two different sizes of InCl$_6$ octahedra (bond disproportionation) and show the multivalent In^{1+} ($5s^2$) and In^{3+} ($5s^0$) valence skip configuration. Note that In s and Cl p orbitals are well separated in the energy window and small hybridization between them is realized. Since Cl p orbital has higher energy than F p orbital, hybridization between In s and Cl p_σ orbitals is somewhat bigger than that between In s and F p_σ obitals. However the hybridization between In s and Cl p is still quite small, hence the ligand hole pairs condensation scenario is safely ruled out and valence/charge disproportionation is clearly realized. Interestingly, two s bands originating from In^{1+} and In^{3+} atoms are almost flat (their bandwidths are smaller than 1 eV) and are located at near the Fermi level and ~4 eV, respectively. For KInF$_3$, RbInF$_3$, and CsInF$_3$ compounds, their candidate structures with space groups of $P\bar{1}$-b and $C2/m$-b have symmetrically equivalent In atoms in the unit cell. Therefore, valence/charge disproportionation is not possible in their candidate structures. Alkali metal (K, Rb, Cs) and Cl atoms strongly have the valence states of 1+ and 1-, respectively, leading for In atoms to have 2+ valence state. The insulating mechanism of these compounds is essentially same as one discussed in LiInF$_3$, and the band gap is formed between the fully occupied
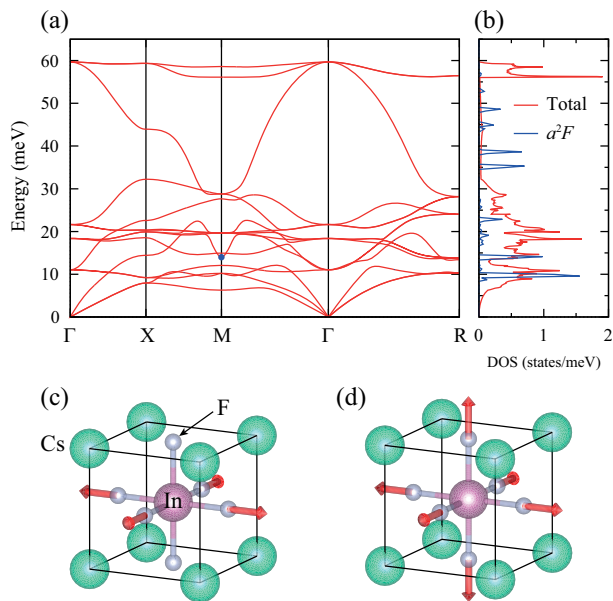
FIG. 8. (Color Online) (a) Phonon dispersion and (b) the corresponding phonon density of state and the Eliashberg function $a^2F(\omega)$ of 0.5 hole-doped cubic $Pm\bar{3}m$-CsInF$_3$ under pressure $P = 32$ GPa ($a = 4.233$ Å). The unit cell of cubic $Pm\bar{3}m$-CsInF$_3$ is shown in (c) and (d). The arrows in (c) and (b) show phonon normal modes at $q = M$ and R, respectively, having the significant electron-phonon coupling constant. The phonon normal mode having the largest electron-phonon coupling strength $\lambda_{q\nu}$ is the F stretching phonon mode shown in (c) and the size of $\lambda_{q\nu}$ is marked by a blue circle in (a).

TABLE III. Phonon related physical parameters for 0.5 hole-doped simple cubic CsInF$_3$ under pressure $P = 32$ GPa. The reduced electron-phonon matrix element (REPME), the total electron-phonon coupling λ, the average phonon frequency $\omega_{\log}$, and the superconducting transition temperature T_c are evaluated in both GGA and HSE06 methods. The REPME is obtained for the F stretching mode shown in Fig. 8(c), which is the most important vibration mode. The temperature T_c is estimated by using the McMillan-Allen-Dynes formula[68] with $\mu^* = 0.10$. T_c with $\mu^* = 0.15$ is also provided in the parentheses. Note that the temperature T_c is not sensitive to μ^* within the confidence interval ranged from 0.10 to 0.15.

	GGA	HSE06
REPME (eV/Å)	5.00	6.95
λ	1.80	3.48
$\omega_{\log}$ (K)	157	124
T_c (K)	21 (18)	24 (22)

$ss\sigma$ bonding and totally empty $ss\sigma^*$ anti-bonding states.

As discussed earlier, all AInX$_3$ (A = alkali metals, X = F or Cl) compounds have the insulating behavior with a significant band gap of approximately 4 eV (based on the mBJ method). Hence, these compounds are not suitable for photovoltaic materials (appropriate band gap size is ranged from 1 to 2 eV) without any band gap tuning like, for example, applying strain or pressure.

Now, we discuss the possible superconductivity in these new In compounds. As shown in Fig. 6, hole doping gives the higher electronic density of states than electron doping in both LiInF$_3$ and CsInF$_3$. Therefore, hole doping would be expected to give higher superconducting transition temperature T_c than electron doping.

We calculated the electron-phonon coupling constant λ in 10 % hole-doped $I4/mmm$-a LiInF$_3$. We found that $\lambda = 0.324$ and the logarithmic average phonon frequency $\omega_{log} = 304$ K. It gives the superconducting transition temperature $T_c = 0.293$ (0.02) K when we used the effective Coulomb repulsion parameter $\mu^* = 0.10$ (0.15) in the McMillan-Allen-Dynes formula[68].

The emergence of superconductivity was reported in charged doped cubic perovskite BaBiO$_3$[56] and CsTiX$_3$ (X = F or Cl)[26] materials. Therefore, the simple cubic perovskite CsInF$_3$ ($Pm\bar{3}m$; No. 221) is also tested for possible superconductivity. At ambient pressure, it

is mechanically unstable with imaginary phonon softening at X and R points (not shown) even with sufficient doping. The unstable phonon mode at R point is the InF$_6$ octahedron breathing mode as shown in Fig. 8(d). With sufficient doping and at high pressure, the structure distortions and valence disproportionation realized in CsInF$_3$ (the second row of Fig. 1) could be suppressed and CsInF$_3$ crystallizes in the simple cubic perovskite structure accompanied by entering the metallic phase. It bears a close resemblance to the phase diagram of BaBiO$_3$[59,61].

Figure 8(a) shows the phonon dispersion of 0.5 hole-doped cubic perovskite CsInF$_3$ under pressure of $P = 32$ GPa (Hole-doped CsInF$_3$ is possible through a certain amount of oxygen substitution for fluorine, for example, CsIn(F$_{1-x}$O$_x$)$_3$, or Cs vacancy could introduce hole doping). The F vibrational mode has the highest energy due to its small mass. However, at particular phonon momentum q (especially at $q = M, R$), this F vibrational mode shows quite significant phonon softening indicating fairly large electron-phonon coupling. The phonon momentum q and mode ν dependent electron-phonon coupling strength $\lambda_{q\nu}$ are 7.24 and 0.19 for the soft phonon modes shown in Figs. 8(c) and (d), respectively. The (total) electron-phonon coupling constant λ is 1.80 and the logarithmic average phonon frequency $\omega_{log} = 157$ K. The McMillan-Allen-Dynes formula[68] with $\mu^* = 0.10$ (0.15) gives $T_c = 21$ (18) K.

Conventional electronic descriptions based on LDA/GGA underestimates the electron-phonon coupling constant λ in Ba$_{1-x}$K$_x$BiO$_3$ and fail to explain its high-temperature superconductivity[69]. Yin et $al.$ found that static correlation (which is captured within GW or hybrid HSE06 functional) enhances the electron-phonon coupling constant λ and describes the transition temperature T_c properly[56]. Motivated by the above study[56], the effect of static correlation on superconductivity in CsInF$_3$ is also tested. Since the F stretching phonon mode (Fig. 8(c)) is the most important to account for

superconductivity, we calculated a reduced electron-phonon matrix element (REPME)[56] for the phonon mode. Table III shows that static correlation enhances the REPME by a factor of ~ 1.4 and gives rise to larger electron-phonon coupling constant $\lambda = 3.48$ and $T_c \approx 24$ K. These results encourage the pursuit of experimental synthesis.

V.   SUMMARY AND CONCLUSIONS

Using computational methods we identified nine new In compounds $AInX_3$ (A = alkali metals, X = F or Cl) and investigated their crystal structures and physical properties. Two distinct insulating mechanisms are realized in the new In compounds. For the compounds that have different sizes of InX_6 octahedra (bond disproportionation), which are $CsInF_3$, $LiInCl_3$, and $NaInCl_6$, they show multivalent In^{3+} ($5s^0$) and In^{1+} ($5s^2$) valence skip configuration. The insulating phase is induced from bond and valence disproportionation. The other In compounds, $AInF_3$ (A = Li, Na, K, Rb) and $AInCl_3$ (A = K, Rb, Cs), have symmetrically equivalent In sites in their unit cell and hence both bond and valence disproportionation are not possible. These In compounds have the divalent valence state of In, which is very rare but thermodynamically stable. In these compounds, two adjacent In atoms are dimerized to produce $ss\sigma$ bonding and $ss\sigma^*$ antibonding states. Each s-electron in In^{2+} completely fills the $ss\sigma$ bonding states. Therefore, the band gap sizes in these compounds indicate the splitting between $ss\sigma$ bonding and $ss\sigma^*$ antibonding states.

These compounds are a new arena for investigating charge, valence, and bond disproportionation. They are similar to the $CsTlX_3$ (X = F or Cl), which had also been predicted theoretically and synthesized experimentally[25,26], but do not have the toxicity problems associated with Tl, and therefore can be synthesized more easily. All these $AInX_3$ compounds are insulators with a sizable indirect band gap of the order of ~ 4 eV, which makes them unsuitable for photovoltaic materials. We also studied the possible superconductivity in these new In compounds. With sufficient doping and at high pressure, $CsInF_3$ crystallizes in the simple cubic perovskite structure and has significant superconducting transition temperature $T_c \approx 24$ K.
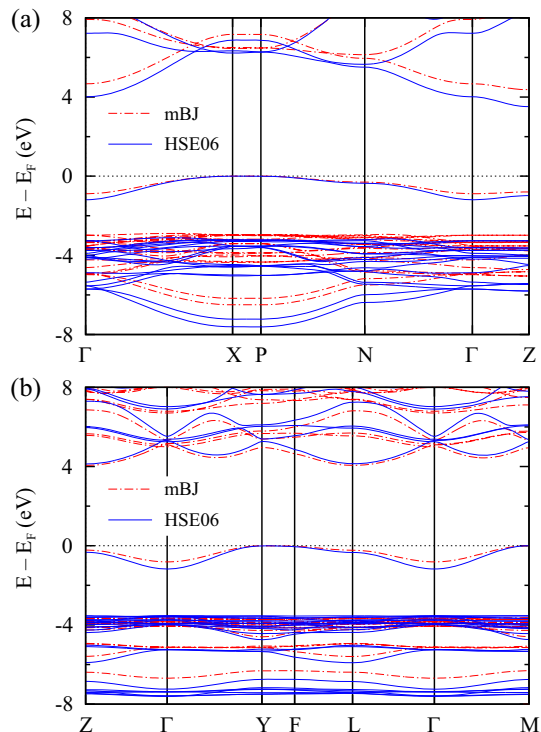
ACKNOWLEDGMENTS

FIG. 9. (Color Online) Comparison between mBJ and HSE06 methods for (a) $I4/mmm$-a $LiInF_3$ and (b) $C2/m$-a $CsInF_3$. Both mBJ and HSE06 methods give the similar band gap.

VI.   APPENDIX

We have estimated band gaps of the semiconducting systems within the mBJ method. In Appendix, we discuss the computational validity of the mBJ method. For the semiconducting systems, the mBJ method is efficient to improve the band gap but is empirical. On the other hand, the rather computationally expensive HSE06 method is well physically constructed and is more accurate on this aspect. Here, we compute the electronic structure within the HSE06 method and compare it with the mBJ method.

Figure 9 shows the comparison between the mBJ and HSE06 methods for two representative electronic structures of $I4/mmm$-a $LiInF_3$ and $C2/m$-a $CsInF_3$. For $I4/mmm$-a $LiInF_3$, mBJ and HSE06 methods give indirect band gaps of 4.37 and 3.51 eV, respectively. In addition, both give indirect band gaps of 4.06 and 4.15 eV, respectively, for $C2/m$-a $CsInF_3$. Since both mBJ and HSE06 methods give the similar band gap for the semiconducting systems investigated in this study, the band gaps estimated from the mBJ method are reliable.

* ck620@physics.rutgers.edu

[1] D. Duan, Y. Liu, F. Tian, D. Li, X. Huang, Z. Zhao, H.

Yu, B. Liu, W. Tian, and T. Cui, Sci. Rep. **4**, 6968 (2014).

[2] A. P. Drozdov, M. I. Eremets, and I. A. Troyan, arXiv:1412.0460 (2014).

[3] A. P. Drozdov, M. I. Eremets, I. A. Troyan, A. Ksenofontov, and S. I. Shylin, Nature (London) **525**, 73 (2015).

[4] I. Errea, M. Calandra, C. J. Pickard, J. Nelson, R. J. Needs, Y. Li, H. Liu, Y. Zhang, Y. Ma, and F. Mauri, Phys. Rev. Lett. **114**, 157004 (2015).

[5] Y. Ge, F. Zhang, and Y. Yao, Phys. Rev. B **93**, 224513 (2016).

[6] J. H. Shim, K. Haule, and G. Kotliar, Phys. Rev. B **79**, 060501(R) (2009).

[7] N. Katayama, K. Kudo, S. Onari, T. Mizukami, K. Sugawara, Y. Sugiyama, Y. Kitahama, K. Iba, K. Fujimura, N. Nishimoto, M. Nohara, and H. Sawa, J. Phys. Soc. Jpn. **82**, 123702 (2013).

[8] C.-J. Kang, T. Birol, and G. Kotliar, Phys. Rev. B **95**, 014511 (2017).

[9] X. Zhang, L. Yu, A. Zakutayev, and A. Zunger, Adv. Funct. Mater. **22**, 1425 (2012).

[10] F. Yan, X. Zhang, Y. G. Yu, L. Yu, A. Nagaraja, T. O. Mason, and A. Zunger, Nat. Commun. **6**, 7308 (2015).

[11] R. Gautier, X. Zhang, L. Hu, L. Yu, Y. Lin, T. O. L. Sunde, D. Chon, K. R. Poeppelmeier, and A. Zunger, Nat. Chem. **7**, 308 (2015).

[12] Q. Hu, D. Y. Kim, W. Yang, L. Yang, Y. Meng, L. Zhang, and H.-K. Mao, Nature **534**, 241 (2016).

[13] Y.-L. Li, S.-N. Wang, A. R. Oganov, H. Gou, J. S. Smith, and T. A. Strobel, Nat. Commun. **6**, 6974 (2015).

[14] X. Dong, A. R. Oganov, A. F. Goncharov, E. Stavrou, S. Lobanov, G. Saleh, G.-R. Qian, Q. Zhu, C. Gatti, V. L. Deringer, R. Dronskowski, X.-F. Zhou, V. B. Prakapenka, Z. Konôpková, I. A. Popov, A. I. Boldyrev, and H.-T. Wang, Nat. Chem. **9**, 440 (2017).

[15] S. Curtarolo, G. L. W. Hart, M. B. Nardelli, N. Mingo, S. Sanvito, and O. Levy, Nat. Mater. **12**, 191 (2013).

[16] J. E. Saal, S. Kirklin, M. Aykol, B. Meredig, and C. Wolverton, JOM **65**, 1501 (2013).

[17] K. T. Butler, J. M. Frost, J. M. Skelton, K. L. Svane, and A. Walsh, Chem. Soc. Rev. **45**, 6138 (2016).

[18] A. Jain, Y. Shin, and K. A. Persson, Nat. Rev. Matter. **1**, 15004 (2016).

[19] A. Jain, K. A. Persson, and G. Ceder, APL Mater. **4**, 053102 (2016).

[20] K. T. Butler, D. W. Davies, H. Cartwright, O. Isayev, and A. Walsh, Nature **559**, 547 (2018).

[21] C. M. Varma, Rev. Mod. Phys. **48**, 219 (1976).

[22] G. E. Eperon, G. M. Paternò, R. J. Sutton, A. Zampetti, A. A. Haghighirad, F. Cacialli, and H. J. Snaith, J. Mater. Chem. A **3**, 19688 (2015). (DOI: 10.1039/c5ta06398a)

[23] M. R. Filip and F. Giustino, J. Phys. Chem. C **120**, 166 (2016).

[24] S. Körbel, M. A. L. Marques, and S. Botti, J. Mater. Chem. C **4**, 3157 (2016).

[25] M. Retuerto, T. Emge, J. Hadermann, P. W. Stephens, M. R. Li, Z. P. Yin, M. Croft, A. Ignatov, S. J. Zhang, Z. Yuan, C. Jin, J. W. Simonson, M. C. Aronson, A. Pan, D. N. Basov, G. Kotliar, and M. Greenblatt, Chem. Mater. **23**, 4071 (2013).

[26] Z. P. Yin and G. Kotliar, EPL **101**, 27002 (2013).

[27] R. J. Cava, B. Batlogg, J. J. Krajewski, R. Farrow, L. W. Rupp Jr, A. E. White, K. Short, W. F. Peck, and T. Kometani, Nature **332**, 814 (1988).

[28] J. A. J. Pardoe and A. J. Downs, Chem. Rev. **107**, 2 (2007).

[29] P. P. Fedorov, A. I. Popov, and R. L. Simoneaux, Russ. Chem. Rev. **86**, 240 (2017). (doi: 10.1070/RCR4609)

[30] R. L. Davidovich, P. P. Fedorov, and A. I. Popov, Rev. Inorg. Chem. **36**, 105 (2016). (doi: 10.1515/revic-2015-0019)

[31] R. Adler, C.-J. Kang, C.-H. Yee, and G. Kotliar, Rep. Prog. Phys. in press (2018). (https://doi.org/10.1088/1361-6633/aadca4)

[32] S. M. Woodley and R. Catlow, Nat. Mater. **7**, 937 (2008).

[33] A. Jain, S. P. Ong, G. Hautier, W. Chen, W. D. Richards, S. Dacek, S. Cholia, D. Gunter, D. Skinner, G. Ceder, and K. A. Persson, APL Materials **1**, 011002 (2013).

[34] https://www.materialsproject.org/

[35] S. Kirklin, J. E. Saal, B. Meredig, A. Thompson, J. W. Doak, M. Aykol, S. Rühl, and C. Wolverton, npj Computational Materials **1**, 15010 (2015). (doi:10.1038/npjcompumats.2015.10)

[36] http://www.oqmd.org/

[37] W. Setyawan, R. M. Gaume, S. Lam, R. S. Feigelson, and S. Curtarolo, ACS Comb. Sci. **13**, 382 (2011).

[38] http://aflowlib.org/

[39] A. R. Oganov and C. W. Glass, J. Chem. Phys. **124**, 244704 (2006).

[40] C. W. Glass, A. R. Oganov, and N. Hansen, Comput. Phys. Commun. **175**, 713 (2006).

[41] G. Kresse and J. Furthmüller, Comput. Mater. Sci. **6**, 15 (1996).

[42] G. Kresse and J. Furthmüller, Phys. Rev. B **54**, 11169 (1996).

[43] J. P. Perdew, K. Burke, and M. Ernzerhof, Phys. Rev. Lett. **77**, 3865 (1996).

[44] P. E. Blöchl, Phys. Rev. B **50**, 17953 (1994).

[45] G. Kresse and D. Joubert, Phys. Rev. B **59**, 1758 (1999).

[46] G. Hautier, S. P. Ong, A. Jain, C. J. Moore, and G. Ceder, Phys. Rev. B **85**, 155208 (2012).

[47] L. Wang, T. Maxisch, and G. Ceder, Phys. Rev. B **73**, 195107 (2006).

[48] A. Jain, G. Hautier, S. P. Ong, C. J. Moore, C. C. Fischer, K. A. Persson, and G. Ceder, Phys. Rev. B **84**, 045115 (2011).

[49] S. P. Ong, L. Wang, B. Kang, and G. Ceder, Chem. Mater. **20**, 1798 (2008).

[50] P. Blaha, K. Schwarz, G. K. H. Madsen, D. Kavasnicka, and J. Luitz, $Wien2k$ (Karlheinz Schwarz, Technische Universitat Wien, Austria, 2001).

[51] F. Tran and P. Blaha, Phys. Rev. Lett. **102**, 226401 (2009).

[52] S. Baroni, S. de Gironcoli, A. D. Corso, and P. Giannozzi, Rev. Mod. Phys. **73**, 515 (2001).

[53] P. Giannozzi *et al.*, J. Phys. Condens. Matter **21**, 395502 (2009).

[54] K. Lejaeghere *et al.*, Science 351, 1415 (2016).

[55] http://materialscloud.org/sssp/

[56] Z. P. Yin, A. Kutepov, and G. Kotliar, Phys. Rev. X **3**, 021011 (2013).

[57] A. V. Krukau, O. A. Vydrov, A. F. Izmaylov, and G. E. Scuseria, J. Chem. Phys. **125**, 224106 (2006).

[58] We have performed USPEX simulations for several $AInX_3$ materials including $LiInF_3$, $RbInF_3$, $CsInF_3$, $LiInCl_3$, $RbInCl_3$, and $CsInCl_3$. After the USPEX simulations, we have collected crystal structures that the energy difference from the lowest energy is within 10 meV/atom for each material and made a structure set as shown in Fig. 1.

[59] D. E. Cox and A. W. Sleight, Solid State Commun. **19**, 969 (1976).

[60] G. Thornton and A. J. Jacobson, Acta Cryst. **B34**, 351 (1978).

[61] D. E. Cox and A. W. Sleight, Acta Cryst. **B35**, 1 (1979).

[62] A. F. Orchard and G. Thornton, J. Chem. Soc. Dalton Trans. **0**, 1238 (1977).

[63] K. Foyevtsova, A. Khazraie, I. Elfimov, and G. A. Sawatzky, Phys. Rev. B **91**, 121114(R) (2015).

[64] A. Khazraie, K. Foyevtsova, I. Elfimov, and G. A. Sawatzky, Phys. Rev. B **97**, 075103 (2018).

[65] G. M. Dalpian, Q. Liu, J. Varignon, M. Bibes, and A. Zunger, Phys. Rev. B **98**, 075135 (2018).

[66] The charge density difference between In^{1+} and In^{3+} atoms in $C2/m$-$CsInF_3$ is small (~ 0.21 e) in the DFT calculations. Note that there is no real difference in d occupations even in well-known charge-order transition metal oxides. See the Ref. [67] in more detail.

[67] Y. Quan, V. Pardo, and W. E. Pickett, Phys. Rev. Lett. **109**, 216401 (2012).

[68] P. B. Allen and R. C. Dynes, Phys. Rev. B **12**, 905 (1975).

[69] V. Meregalli and S. Y. Savrasov, Phys. Rev. B **57**, 14453 (1998).